A new simple h-mesh adaptation algorithm for standard Smagorinsky LES: a first step of Taylor scale as a refinement variable

Sayan Kaennakham[1], Arne E. Holdø[2] and Caroline Lambert[3]
[1] Energy Technology Applied Research Group, Faculty of Engineering and Computing, Coventry University, CV15FB, U.K.
kaennaks@coventry.ac.uk
[2] Narvik University College, Postboks 385, 8505 Narvik, NORWAY
ArneErik.Holdo@hin.no
[3] Department of Systems Engineering, Coventry University, CV15FB, U.K.
cex455@coventry.ac.uk

ABSTRACT
The interaction between discretization error and modeling error has led to some doubts in adopting Solution Adaptive Grid (SAG) strategies with LES. Existing SAG approaches contain undesired aspects making the use of one complicated and less convenient to apply to real engineering applications. In this work, a new refinement algorithm is proposed aiming to enhance the efficiency of SAG methodology in terms of simplicity in defining, less user's judgment, designed especially for standard Smagorinsky LES and computational affordability. The construction of a new refinement variable as a function of the Taylor scale, corresponding to the kinetic energy balance requirement of the Smagorinsky SGS model is presented. The numerical study has been tested out with a turbulent plane jet in two dimensions. It is found that the result quality can be effectively improved as well as a significant reduction in CPU time compared to fixed grid cases.

1. INTRODUCTION

One of the serious disadvantages of using fixed grids for solving complex Computational Fluid Dynamics (CFD) problems is that the grid points are generated and distributed in the domain before any details on the nature of the solution are known. As a result, time and computational cost are normally required to ensure mesh independence. Moreover, the task of distributing the mesh normally requires knowledge of the flow problem at hand. In other words, a proper design of the mesh requires a good understanding of the fluid dynamics being investigated. The main objective of developing Solution Adaptive Grid (SAG), also known as Dynamic Grid Adaptation (DGA), method is to alleviate this problem.

Two most and common used refinement strategies are mesh moving or r-refinement and h-refinement. The former based on the idea of fixing the number of grid points and allowing the grid points to move accordingly to some selected 'mesh driving' function in order to capture the main flow feature. In h-refinement on the other hand allows the number of grid points to vary. Nodes are added in to regions of interest, normally those with high gradient of flow parameters and/or taken from where high mesh density is no longer needed.

It is unfortunate not to be able to say which refinement strategy is more superior. Nevertheless, despite a number of choices available in r-refinement family, the necessity of

solving additional mesh driving functions which introduces extra requirement of computational memory storage together with the lack of reliable and high requirement for users' input robust monitor or weight function for broader range of flow problems have accordingly made this mesh refinement strategy relatively less attractive and for this reason in this work we focus on h-refinement type.

Without any additional functions to drive the mesh in h-refinement, the means of identifying the regions of interest for performing mesh adaptation are crucial. Ideally, these regions should be provided by a method of error measurements. However, the nonlinearity of the governing Navier-Stokes equations, together with additional transport equations makes this task not easy to handle. Many researcher have made use of error estimators, available from Richardson extrapolation-based [1] to interpolation-based [2]. General downside of adopting grid adaptation algorithm involving error estimator is that it relies on the smoothness of the differential equation, singularity in case of discontinuous flows. This is known to be remediable by grid smoothing procedure and as a result, the grid adaptation near discontinuities is readily driven by the grid smoothing procedure rather than the error estimator itself [3,4]. Alternatively to this, the use of error indicators, generally based on large flow gradients, also receives attentions from recent grid adaptation researches. Even thought this indicator is straightforward and simple to implement, it must be noted that continuous local refinement based on local dominant flow feature does not always reduce certain measures of the global error [5-7]. This indicates that difficulties can arise in selecting a robust match between error indicator formulation and its accordingly chosen flow parameters, referred to as refinement variables. Next to this is the attempt to control the variation of the chosen region of interest identification mean over the domain and is generally done by adopting a normalization method and once again, a well-defined one is important to efficiently represent local error compared to the global one. Furthermore, in order to prevent the algorithm from producing too small elements, and therefore redundant cells, a users' judgment in controlling the size of the smallest elements generated is also required.

In CFD, while there is a large number of studies of mesh adaptation applied to compressible and Euler flows [8-17], it is interesting to see such a relatively small number of work done in the area of incompressible flows, [18,19], particularly flows with high Reynolds number [20-22]. This feature can be explained by the complication of numerically solving Navier-Stokes' equations plus special treatments to account for turbulent mechanism where finer mesh no longer always leads to higher result accuracy as very often encountered in the use of large eddy simulation (LES).

Resulting from the principal concept of large eddy simulation (LES) in which turbulent scales are decomposed by the filtering process, the original governing equations contain extra terms and require subgrid scale (SGS) model. The quality assessment of LES is then determined by two main sources of error, numerical discretization error and modeling error and they are both characterized by the grid resolution. This implies that the choice of defining grid resolution is effectively crucial. Studied by many authors [23,24], for classical or implicit filtering LES, refining the mesh and hence increasing the grid resolution results in more small scales to be resolved and thus further decreasing the effect of the SGS. This phenomenon remains until the mesh size is comparable to the smallest turbulent scale namely Kolmogorov scales and the LES process then loses its identity and becomes DNS. As pointed out also by Vreman et al. [25], the two types of error may partially cancel each other and as a consequence grid refinement may not necessarily lead to better LES result. This feature introduces some uncertainties in applying existing refinement algorithm whose main aims are to decrease only the discretization error. All these negative features encourage modern researchers to come up

with new alternatives of mesh refinement algorithm and one of the main objectives of this work is focused on this problem.

In this work we propose a new mesh refinement algorithm that is simple to implement, requiring little user interventions, judgments, and priory knowledge of the problem being investigated, no normalizations means needed, no element size thresholds required, specifically designed for standard LES simulation of high Reynolds number flows, relatively computationally cheap and capable of providing satisfactory results. The new refinement variable proposed in this work is a function of a real physical scale of turbulence known as the Taylor scale. It is formulated aiming to link the benefit of using SAG to the natural feature of the chosen turbulent model, classical large eddy simulation (LES) with the standard Smagorinsky subgrid scale model, based on the production and dissipation of energy balance assumption. To the authors' knowledge, this is the first time in study of SAG to bridge together the three branches; solution adaptive grid methodology, real physical turbulent scales and the nature of the chosen Smagorinsky subgrid scale model.

2. THEORETICAL BACKGROUND

2.1. FINITE VOLUME-LARGE EDDY SIMULATION (FV-LES)

The main feature of LES is the division of turbulent scales, the larger from the smaller. The larger ones are to be explicitly calculated by the mesh while the smaller ones are modelled by a subgrid scale (SGS) model. The process of separating the scales is called 'space filtering' and it can be done in either Fourier (wave-number) space or physical space.

There are two ways of filtering or decomposing the scales or eddies of turbulence in LES; explicit and implicit. The former requires an explicit form of a filtering operator with a specific filter width (denoted by Δ, normally related to the grid spacing (h)) available from the top-hat filter, Gaussian filter and sharp cut-off filter [26]. The latter is carried out in such a way that the governing equations are directly solved assuming that the larger scales are calculated by the discrete representation nature of the selected numerical discretization method. By doing this, it is automatically assumed that $\Delta \approx h$.

In finite volume type, as used in this study, a volume-averaging operation similar to Schumann [27] of a flow parameter **f** is employed, defined as follows.

$$\overline{f} = \frac{1}{\Delta x \Delta y \Delta z} \int_{\Delta x} \int_{\Delta y} \int_{\Delta z} f(x^*, y^*, z^*)\, dx^*\, dy^*\, dz^* \tag{1}$$

With the Gauss's divergence theorem that links the volume integrals to the surface integrals and by part integration technique, the (implicitly) filtered governing equations can be written as.

$$\overline{\mathrm{div}\, u} = \delta_j\, {}^j\overline{u}_j \tag{2}$$

$$\frac{\partial \overline{u}_I}{\partial t} + \delta_j({}^j\overline{u}_j\, {}^j\overline{u}_I) = -\delta_i\, {}^j\overline{p} + \delta_j\left(\nu\, {}^j\overline{\frac{\partial u_i}{\partial x_j}} - \tau_{ij}\right) \tag{3}$$

Where τ_{ij} is the subgrid-scale stress and is defined as.

$$\tau_{ij} = {}^j\overline{u_i u_j} - {}^j\overline{u_i}\, {}^j\overline{u_j} \tag{4}$$

Where $j_{\bar{\varnothing}}$ denotes the mean, surface-averaged value of a flow parameter ϕ over the surface in which its normal vector is in j –direction and δ_j is the usual finite difference operator. In LES, the subgrid-scale stress needs to be modelled by the use of a subgrid-scale model (SGS).

2.2. SMAGORINSKY SUBGRID SCALE MODEL

The Smagorinsky model [28] uses the concept of an eddy viscosity to relate the subgrid-scale turbulent stresses, τ_{ij}, to the rate of strain of the resolved velocity field, $\bar{S}_{ij}$ by the following form.

$$\tau_{ij} - \frac{1}{3}\tau_{kk}\delta_{ij} = -2\upsilon_t \bar{S}_{ij} \tag{5}$$

$$\bar{S}_{ij} = \frac{1}{2}\left(\frac{\partial \bar{u}_i}{\partial x_j} + \frac{\partial \bar{u}_j}{\partial x_j}\right) \tag{6}$$

Assuming the balance of production and dissipation of the turbulence kinetic energy in the inertial subrange region on the energy spectrum, and with the use of the dimensional analysis, Smagorinsky proposed a calculation of υ_t by;

$$\upsilon_t = (C_2\Delta)^2 \,|\, \bar{S} \,|\, \tag{7}$$

Where $\bar{S} = (2\bar{S}_{ij}\,\bar{S}_{ij})^{\frac{1}{2}}$ and Δ denotes the subgrid length scale associated with the grid size, h $(= (\Delta x \Delta y \Delta z)^{\frac{1}{2}})$. The Smagorinsky constant C_s is found to be problem-dependent and for a study of free shear flow as in this work, $C_2 = 0.1$ is used for all the simulations.

2.3. TURBULENCE SCALES AND TAYLOR SCALE

In study of turbulence there are three most often referred to scales : the integral length scale (L), the Taylor scale (λ), and the Kolmogorov microscale (η). The first two can be defined using the autocorrelation function, also known as the autocorrelation coefficient (R), expressed as:

$$R_{u'u'}(r) = \frac{\langle u'(x)u'(x+r))\rangle}{\langle (u'(x)u'(x)\rangle} \tag{8}$$

Where the $\cdot\langle - \rangle$ represents time averaged values, u′ (x) is the velocity fluctuation at point x and with r being a distance away from that point. The second derivative of the autocorrelation function at the origin can be used to define the Taylor scale (λ), expressed as.

$$\left.\frac{\partial^2 R}{\partial r^2}\right|_{r=0} = -\frac{2}{\lambda^2} \tag{9}$$

Following the first Kolmogorov hypothesis, the smallest turbulence scale known as Kolmogorov length and time scale can now be written respectively as;

$$\eta = \left(\frac{\upsilon^3}{\varepsilon}\right)^{1/4}, \quad \tau = \left(\frac{\upsilon}{\varepsilon}\right)^{1/2} \tag{10}$$

In the framework of isotropic and homogenous turbulence studies, it is common to define the Taylor scale and assume the dissipation rate (ε) as a function of the Taylor scale.

$$\lambda^2 = \frac{\left\langle u^2 \right\rangle}{\left\langle \left(\frac{\partial u'}{\partial x_1} \right)^2 \right\rangle} \quad \Rightarrow \quad \varepsilon = 2\upsilon \left\langle \left(\frac{\partial u'}{\partial x_1} \right)^2 \right\rangle = 2\upsilon \frac{\left\langle u^2 \right\rangle}{\lambda^2} \tag{11}$$

Assuming that the production and dissipation of the kinetic energy are equal and following the definition of the Reynolds number characterizing the largest scale of turbulent motion, and with isotropic assumption, the relations between the three turbulent scales can now be related as follows.

$$\frac{\eta}{L} \approx C_1 \left(Re_L^{-\frac{3}{4}} \right), \ \frac{\lambda}{L} \approx C_2 \left(\mathrm{Re}_L^{-\frac{1}{2}} \right) \quad \text{and} \quad \frac{\eta}{\lambda} \approx C_3 \left(\mathrm{Re}_L^{-\frac{1}{4}} \right) \tag{12}$$

Where C_1 are constants. The time scales can also be related in the same way. It can be seen now that the Taylor scale lies somewhere between the other two, $\eta \ll \lambda \ll L$, or in other words, it lies somewhere in the inertial subrange on the energy spectrum.

2.4. NUMERICAL METHOD

The central-difference is adopted to take care of the diffusion term where second-order accuracy can be attained. For the non-linear convection term, we use a second-order-accurate central-differencing scheme i.e. in the momentum equations, the face value of a variable ϕ_f can be calculated as follows:

$$\varnothing_{f,CD} = \frac{1}{2}\left(\varnothing_0 + \varnothing_1\right) + \frac{1}{2}\left(\nabla\varnothing_o \cdot \vec{r}_o + \nabla\varnothing_1 \cdot \vec{r}_1\right) \tag{13}$$

Where the indices refer to the cells that share the face f, see Figure 1. The reconstructed gradients, denoted by ∇, are approximated using the Green-Gauss cell-based method defined as.

$$\left(\nabla\varnothing\right)_{c0} = \frac{1}{V}\sum_f \vec{\varnothing}_f \vec{A}_f \tag{14}$$

$$\vec{\varnothing}_f = \frac{\varnothing_{c0} + \varnothing_{c1}}{2} \tag{15}$$

Using the central-differencing schemes can very often produce unbounded solutions and non-physical wiggles leading to stability problems for the numerical procedure. This problem is overcome with using a deferred approach where the face value is calculated by:

$$\varnothing_f = \underset{\text{implicit}}{\varnothing_{f,UP}} + \underset{\text{explicit}}{\left(\varnothing_{f,CD} - \varnothing_{f,UP}\right)} \tag{16}$$

The upwind part, denoted by UP, is treated implicitly while the difference between itself and the central-difference, denoted by CD, is treated explicitly.

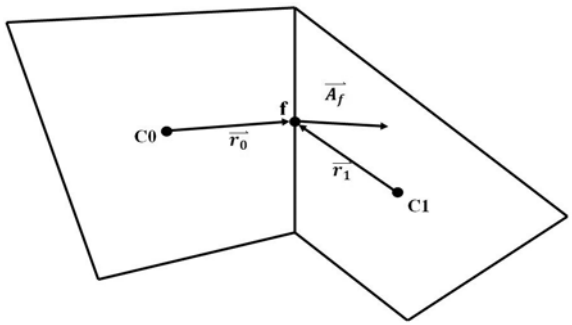

Figure 1. Control volume illustrating the discretization of a scalar transport equation.

For transient simulations, in this work we use a fist-order implicit discretization where all the unknowns are evaluated from the fields for time level n + 1, can be seen in general form as.

$$\int_V \frac{\varnothing^{n+1} - \varnothing^n}{\Delta t} dV + \oint \varnothing^{n+1} \vec{u}^{n+1} \cdot d\vec{A} = \oint \Gamma_{\varnothing}^{n+1} \nabla \varnothing^{n+1} \cdot d\vec{A} - \oint \mathbf{P}^{n+1} \cdot d\vec{A} \tag{17}$$

For a given time step, all the equations are solved iteratively until the convergence criteria are met.

The discretization of the continuity equation proceeds in the similar way to that of the momentum equation. Integrating over a control volume reads;

$$\sum_f^{N_{faces}} M_f A_f = 0 \tag{18}$$

Where $M_f = u_n$ is the mass flux across face f. A linear interpolation is used to link the surface values to the centre ones. This process usually results in unphysical checker-boarding of pressure. To avoid checker-boarding of pressure, a procedure similar to that outlined by Rhie and Chow [29] is employed. The scheme interpolates the pressure values at the face using momentum equation coefficients. Using this procedure, M_f can then be written as.

$$M_f = \rho_f \frac{a_{P,c0} u_{n,c0} + a_{P,c1} u_{n,c1}}{a_{P,c0} + a_{P,c1}} + d_f((P_{c0} + (\nabla P)_{c0} \cdot \vec{r}_0 - (P_{c1} + (\nabla P)_{c1} \cdot \vec{r}_1)) \tag{19}$$

Where P_{c0}, P_{c1} and u_{c0}, u_{c1} are the pressures and normal velocities respectively, within the two cell sharing the face and $\hat{M}_f$ contains the influence of velocities in these cells.

In the linearization process, each discrete equation will be linearized implicitly with respect to that equation's dependent variable. This results in a system of linear equations with one equation for each cell in the domain. A point implicit (Gauss-Seidel) linear equation solver is used in conjunction with an algebraic multigrid (AMG) method to solve the resultant scalar system of equations for the dependent variable in each cell. Pressure-velocity coupling is achieved by using a well-known semi-implicit method for pressure linked equations (SIMPLE) algorithm.

3. MESH REFINEMENT CRITERIA

Successful applications of SAG approach in CFD are strongly dependent on several important factors. Sophisticated and complex algorithms may provide impressive results but at the same time involve some undesired features such as high computational demand to deal with extra terms and users' interfere and judgments. As a consequence, defining a proper refinement algorithm or criteria is very often a compromise between the three components; the computational demand, convenience and simplicity to use and the level of accuracy acceptable.

3.1. THE TAYLOR SCALE AS A REFINEMENT VARIABLE

Lying in the inertial subrange of the energy spectrum where the balance of production and dissipation of kinetic energy assumption takes place is the so-called Taylor scale, denoted by λ. Eqn (12), allows one to globally estimate the Taylor scale from the pre-defined integral length scale and the Reynolds number (Re_t) based on it [30]. To represent local kinetic energy transfer amongst turbulence scales with the use of mesh adaptation approach as the chosen refinement variable however, it has to be approximated locally. For the study of turbulent plane jet as is the case of this work, the attempt of locally estimating the Taylor scale (λ_1) adopted in [31] for turbulent round jet is followed.

$$\frac{\lambda}{\delta} = C^* \, Re_t^{-\frac{1}{2}} \quad \Rightarrow \quad \lambda_i \approx C^* \left[\delta_1 \left(\frac{\delta_1 U_1}{\nu} \right)^{-\frac{1}{2}} \right. \tag{20}$$

With C* being a constant and referred to after as refinement constant, the subscribes, 1, indicate the locally defined property and δ_1 and U_1 are the local characteristic scale and the velocity respectively. Since the Taylor scale was originally defined in statistical means, we replaced U_1 with its time-averaged value. Different values of C^* result in different adaptation behavior and final solution. A primary simulation was run with the standard $k-\varepsilon$ model to provide an approximation of the local characteristic scale δ_1 which was taken to be twice the jet-half width[1].

Unlike in the use of general h-refinement where it is necessary to introduce a normalization of the error indicator in order to prevent a strong change of the raw value of the refinement variable, this study requires no normalization means. Instead, since the main attempt is to adapt the local gird $(\Delta_{mesh1} = (\Delta x \Delta y)^{\frac{1}{2}})$ to meet the same order of magnitude as the local Taylor scale, it straightforwardly follows that a new proposed form of refinement variable, E_t, can be defined as a function of the two parameters.

$$E_1 = f(\lambda_i, \Delta_{mesh,1}) = \frac{\Delta_{mesh,1}}{\lambda_1} = \frac{1}{C^*} \left[\frac{(\Delta x \Delta y) \cdot ((U_1))}{\delta \cdot \upsilon} \right]^{\frac{1}{2}} \tag{21}$$

Defining a refinement variable this way has also an advantage of not needing any users' judgments for refinement bounds, normally required to prevent SAG from generating redundant cells. This is because the ratio can simply be set to vary around the value of unity.

3.2. SOLUTION ADAPTIVE GRID (SAG) ALGORITHM

A simple process of adding and removing the grid points shown in Figure 2 is used with a uniform rectangular shape mesh. The algorithm consists of 5 main steps, listed as:

---

[1] is equal to the y-value where the mean velocity is half the mean centerline velocity of the jet, denoted here as $y_{\frac{1}{2}}$.

1. Calculating the refinement variable defined in Eqn (21), using the initial condition obtained either from the initial condition or the calculation previously carried out, for each control volume all over the domain.
2. Comparing the value obtained from the first step for each cell with the unit value of one. Those calls with $E_l > 1$ are marked and subjected to refinement activity and only one level of refinement is allowed to perform for those cells with $E_l < 1$. Therefore, those cells that require more than one level of refinement are subject to undergo a coarsening process.
3. Performing a mesh adaptation in such a way as shown in Figure 2.
4. Interpolating flow parameters' values from parent to child cells.
5. Continuing the calculation for the next time step.

To maintain accuracy, neighbouring cells are not allowed to differ by more than one level of refinement. This helps preventing the mesh adaptation from generating excessive cell volume variations (reducing truncation error). In addition, this also ensures that the position of the parent (original) and child (refined) cell centroids are similar (reducing errors in the flux evaluations). Using this adaptation scheme, mesh that is coarser than the original ones is not allowed to be generated.

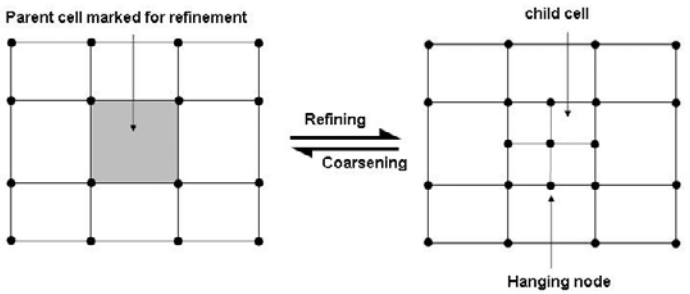

Figure 2. Refining and coarsening process for one level of refinement.

4. APPLICATION WITH A 2D TURBULENT PLANE JET

4.1. PLANE JET SIMULATIONS

Figure 3 illustrates a sketch of a plane jet together with all related parameters. Like other kinds of jets, there are so far only a few numerical simulations done on plane jets. Stanley at al. [32] and Klein et al. [33] have used direct numerical simulation (DNS) to study the mixing structure and the effect of the Reynolds number respectively. Both studies considered a relatively low Reynolds number, 4,000 when compared with existing experimental work. The main factor determining this is mainly the limitation in computer facility. The use of LES allows one to tackle jet simulations with higher Reynolds number as conducted by Ribault et al. [34] with the Reynolds number of 3×10^4 and with different SGS models. They found that the standard Smagorinsky model is excessively dissipative. Recent LES study by Liu et al. [35] at Re = 4,000 used both linear and non-linear SGS models. Even though the results from these testing models do not give any big differences, it is recommended in this work that choosing one that is well-conditioned, efficient, and easy to implement is a better choice. This suggests that a strong influence of computational capability still persists and remains the main factor even for LES simulations and therefore new alternatives to treat high Reynolds number flows should be put forward.

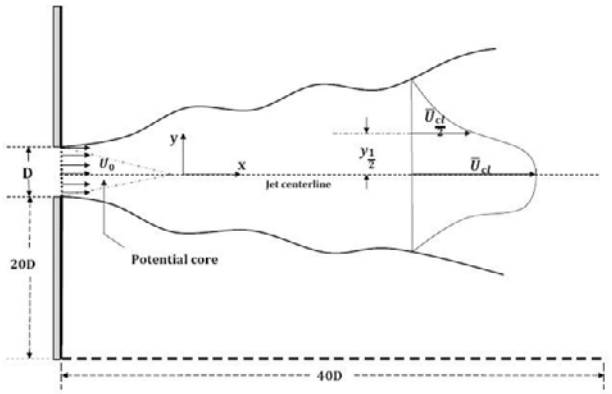

Figure 3. Sketch of a turbulent plane jet with related parameters and dimensions.

4.2. MODEL AND SIMULATION SETUP

4.2.1. Governing equations

The investigation carried out in this work deals with a statistically two-dimensional plane jet, assuming that the third dimension is sufficiently large. The chosen Reynolds number is 4,000, based on the nozzle diameter (D) and the inlet velocity (U_0) in which experimental data is available for validation. Only conservation of mass and momentum were applied as the flow was assumed to be in the incompressible range and without any heat transfer. The governing equations were then discretized using the finite volume as outlined in section (2.3). The time step size was fixed to 0.342 for all simulations and was chosen correspondingly to the Taylor time scale for $C^* = 1$ in Eqn (21).

4.2.2. Computational domain

A 2D computational domain with the size of 40D × 41D, same as those adopted in Klein et al. [33] and Liu et al. [35] is constructed and used for all the simulations. It is one of the wider objectives of this work to investigate the necessity of having extremely fine grids, which is a reason why LES has traditionally been regarded as inaccessible. In using LES with high Reynolds number flows, it is an ideal to have only the locally isotropic smaller dissipative scales being modelled by the SGS model but it is not always practical. For this, the first three conventional simulations were carried out with three different mesh sizes. The fist contains 33,000 cells (referred to as NO-SAG-1) and is termed as vary large eddy simulation (VLES). The medium mesh has 96,000 cells (referred to as NO-SAG-2) and the finest one consists of 133,000 cells (referred to as NO-SAG-3). All the three were constructed based on the information given by Ribault et al. [34] and Klein et al. [33]. In the x-direction, the rectangular mesh was refined in the vicinity of the jet exit and smoothly expanded towards the entrainment and outflow boundary and this is also the case in the lateral direction, see Figure 4(f). This is to ensure that more grid points are placed in the area where high velocity gradients are expected.

For study of application of the proposed mesh adaptation algorithm, a very coarse mesh consisting of 6,800 rectangular-shape cells was generated and used as the initial mesh for SAG application, Figure 4(a). Constructing the initial mesh this way is specifically to demonstrate the efficiency of the algorithm in alleviating the need of a prior knowledge of the flow at hand in meshing process. This is crucial particularly for engineering applications where meshing as well as mesh testing normally requires a lot of efforts in order to reach the aimed result accuracy.

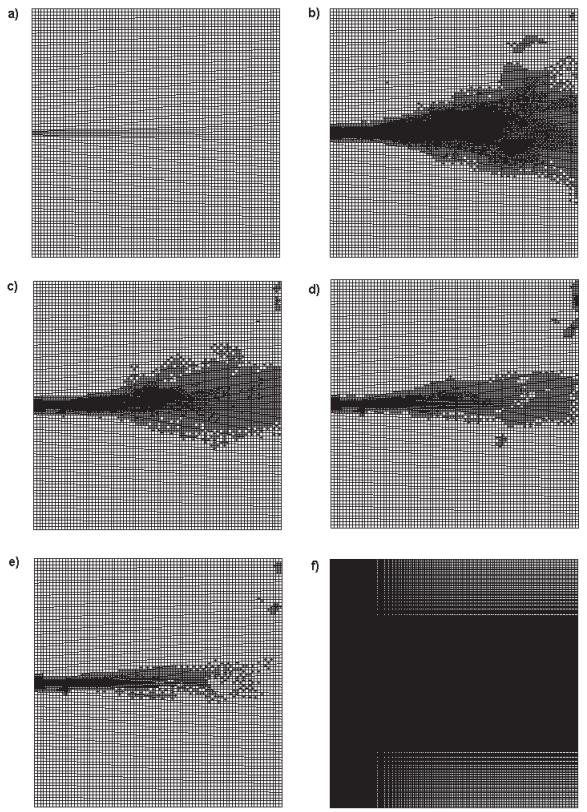

Figure 4. a) Initial mesh for SAG studies (6,800 cells), b) Final mesh for SAG with C* = 2 (31,838 cells), c) Final mesh for SAG with C* = 3 (17,528 cells), d) Final mesh for SAG with C* = 4 (12,830 cells), e) Final mesh for SAG with C* = 5 (10,124 cells) and f) Conventional mesh NO-SAG-2 (96,000 cells).

4.2.3. Inlet and boundary conditions

Following Klein et al. [33], a hyperbolic-tangent velocity profile was constructed and imposed at the inlet, as expressed below.

$$\bar{U} = \frac{U_0}{2} + \frac{U_0}{2} tanh\left(\frac{-|y| + 0.5D}{2\theta}\right), \bar{V} = 0 \tag{22}$$

Where θ is the momentum thickness and is set to D/20. The nature of jet flows which is evolving in both time and space in all directions has made the use of periodic boundary conditions impossible. Instead, for all the outflow sections the conditions were set with zero gauge pressure and the negative velocities normal to each outflow were clipped.

5. RESULTS AND DISCUSSION

The results presented are compared against available measurements of Browne et al. [36] (Re = 3,000), Thomas and Chu [37] (Re = 8,300) and Gutmark and Wyganski (GW) [38] (Re = 30,000)

5.1. DIFFICULTIES IN NUMERICAL STUDY OF A PLANE JET IN 2D.

As studied by Stanley and Sarkar [39] in 1997, as well as those carried out before that, and later pointed out by Stanley et al. [40], numerical work on turbulent plane jets in two dimensional is known not be a success. The absence of spanwise instabilities in two-dimensional simulations leads to a phenomenon that is not seen in experimental work namely 'dipoles', jet breaking down to vortex resulting in incorrect mean velocity profile. Furthermore, not only the 2-D simplification assumed in this work, but the most relevant imperfective assumption to this work is also the zero turbulent level at the inflow which is not feasible in the real experiment. The wide range and scatter between existing experimental measurements has also made the validation of numerical study rather difficult. These all contribute to deviation of the results obtained from this work from the references and should be kept in mind.

5.2. EFFECTS OF THE REFINEMENT CONSTANT.

Based on Eqn (21), the only controlling parameter is the refinement constant C*. The existence of the refinement constant allows one to automatically estimate the smallest scales to be resolved by the mesh and these scales are assumed to appear in the inertial subrange of the energy spectrum. The idea corresponds to the fundamental principal of the standard Smagorinsky SGS model, the balance of the production and dissipation of the kinetic energy. Figure 4 illustrates the mesh distribution and density of all the study cases along with one from the conventional mesh cases. As can be seen, the smaller value of C* give raise in the number of smaller cells meaning that smaller scales are being resolved. When the refinement variable increases, less grid points are added in the far-field region. In all the cases however, relatively higher mesh density still persists in the near-field area whose capability of capturing main flow mechanism has strong effect on the overall accuracy.

Figure 5(left) shows the longitudinal centreline fluctuation intensities obtained from the application of SAG for C* = 5 against the experimental work as well as those from Ribault et al. [34] where the same SGS model was used. It is found that for the near-field, $x < 7D$, the results obtained from the chosen SAG case is under-predicted while with the a good agreement remains for the conventional mesh and the experimental data. With the same SGS model however, the use of SGA algorithm is seen to rapidly enhance the fluctuation intensity for $7D < x < 10D$ and eventually reaches the similarity value at $x = l0D$. Results from the other SAG cases are also in the same trend (not shown). From this figure, values at $x = 11D$

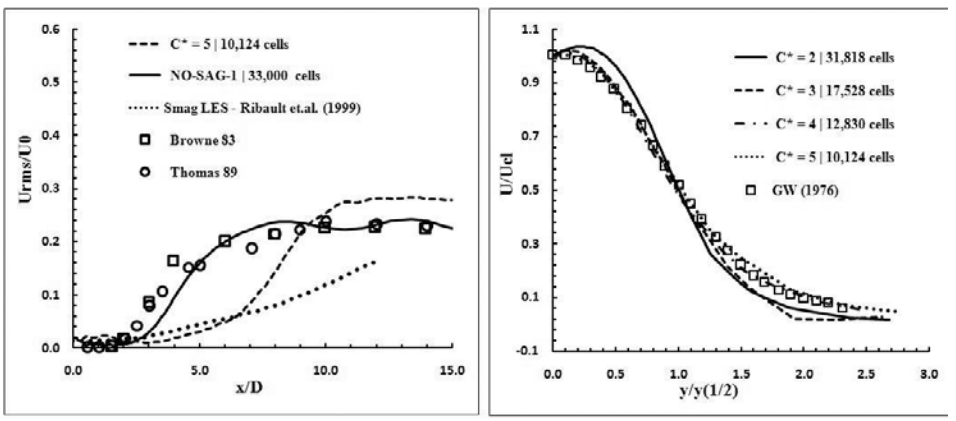

Figure 5. Centreline velocity fluctuation (left) and normalized longitudinal velocities at x=11D (right).

are then chosen for data comparison in which the self-similarity of the fluctuation quantities starts and it is far enough from the outflow boundary. Figure 5(right) confirms the existence of the similarity state at x = 11D of the jet where the normalized velocity profiles of all the SAG cases are in a good agreement with the reference. Most of the comparing data presented in this work is then normalized with the local centreline velocity U_{cl} and the jet half-width $y_{\frac{1}{2}}$.

It is evident from Figure 5(left) that mesh resolution level at the inlet has an important role to play in generating turbulent intensity and thus accounting for the upstream flow dynamic. Even though the inlet velocity profile is imposed with zero level of turbulent, higher mesh resolution is clearly responsible for reproducing the smaller scale turbulent structures. This indicates that without any turbulent structures constructed in artificial manner and imposed at the inlet boundary, the requirement for high mesh resolution persists.

The evolution of the inverse square of the jet velocity at the centreline is shown in Figure 6. It can be seen from the results obtained from conventional mesh NO-SAG-3 that the increase in mesh density can lead to an unexpected result. Those from applying SAG on the other hands, are slightly lower than the measurement and the gap between the two tends to increase with the decrease of C*" . The same trend also occurs for the jet half-width growth downstream as illustrated in Figure 7.

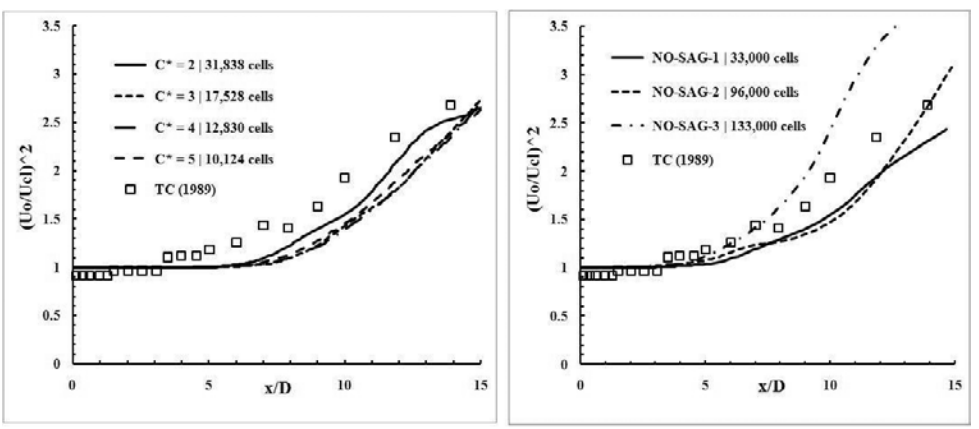

Figure 6. Centreline inverse square of the jet velocity: left) from SAG study, right) from the conventional mesh cases.

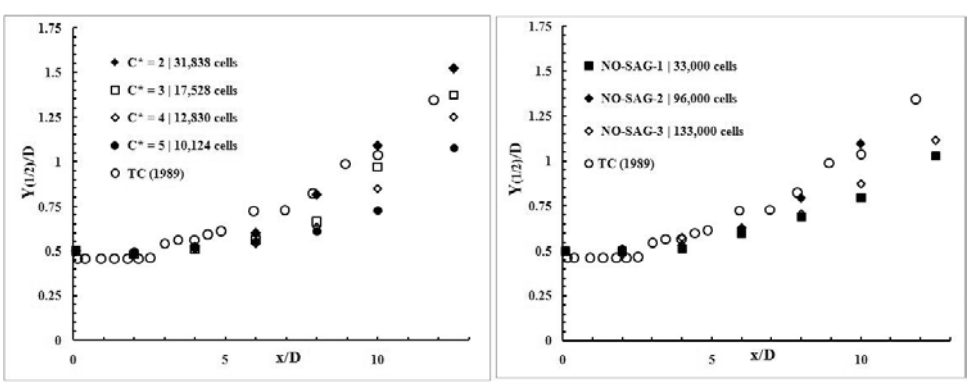

Figure 7. Downstream jet half-width growth ,$y_{\frac{1}{2}}$.

In the self-similar region, the jet half-width $y_{\frac{1}{2}}$ is believed to grow linearly with the distance downstream x, expressed as.

$$\frac{y_{\frac{1}{2}}}{D} = K_1\left(\frac{x}{D} + C_1\right) \tag{23}$$

Furthermore, the well-known similarity relationship for a plane jet defined below is also anticipated.

$$\left(\frac{U_0}{U_{c1}}\right)^2 = K_2\left(\frac{x}{D} + C_2\right) \tag{24}$$

Where K_1, K_2 are the jet spreading and centreline velocity decay rate respectively and their values are shown in Table 1 along with all the referencing works both numerical and experimental. Here an overall agreement can be observed especially for the SAG case with C* = 5. With higher refinement constant, the result reveals a gradual decline in the jet half-width spreading rate whereas a higher centreline decay rate is noticed. This can be explained as the relatively coarser mesh with higher refinement constant particularly at the inlet leads to less turbulent intensity captured in the resolved field and the flow relatively more laminar resulting in a longer potential core region. The same aspect was found in the findings of Goldschmidt and Bradshaw [41] where their result revealed a larger jet-spreading angle for jet with higher exit turbulence intensity.

Table 1. Spreading and centerline velocity decay rates

	K_1	K_2
*C** = 2	0.15	0.16
*C** = 3	0.15	0.18
*C** = 4	0.13	0.18
*C** = 5	0.11	0.19
NO-SAG-1	0.075	0.17
NO-SAG-2	0.091	0.17
NO-SAG-3	0.021	0.45
Browne et al. [36]	0.104	0.143
Thomas and Chu [37]	0.11	0.22
Gutmark and Wygnanski [38]	0.1	0.188
Smagorinsky LES of Liu et al. [35]	0.12	0.20

Figure 8-10 show respectively the normalized transverse velocity, streamwise fluctuation and lateral fluctuation distribution at *x* = 11D. The results are in fairly good agreement with the reference. Once again a better level of overall accuracy is provided by the case with highest value of C* suggesting that finer mesh is not always more effective. The same feature can be found with the case of the finest mesh NO-SAG-3 where the comparatively worst flow parameters approximation is revealed. This could be explained by the nature of the standard Smagorinsky model with comparatively too small grid filtering width. With smaller grid spacing, the turbulent scale to be resolved by the mesh is moving toward higher wave number on the energy spectrum where the energy dissipation takes place. In the fundamental

of the Smagorinsky SGS model however, the SGS viscosity (ν_τ) is defined as a function of the energy dissipation rate per unit mess (ε) and the wave number $(\frac{1}{\Delta})$. These two parameters characterize turbulence scales lying in the inertial subrange and this is where the energy equilibrium (production equals dissipation) is assumed. We then can write $\varepsilon = 2\upsilon_t \bar{S}_{ij} \bar{S}_{ij}$ leading to the approximation of the SGS viscosity as shown in Eqn 7.

For the case with fine mesh, NO-SAG-3 for instance, the smallest grid spacing is found to be of the same of magnitude as the smallest turbulent scales or the Kolmogorov scales. At these scales, (most of) turbulent kinetic energy is dissipated to heat by viscous effect and therefore the principal concept and assumption of estimating the SGS viscosity as explained above for the Smagorinsky model is no longer valid leading to undesired high level of modeling error and evidently from this study, this error can contaminate the overall accuracy. It is clear that even though the numerical error can possibly be reduced by reducing the mesh size, the modeling error cannot be overlooked. As pointed out by Klein [42] even though grid refinement is not

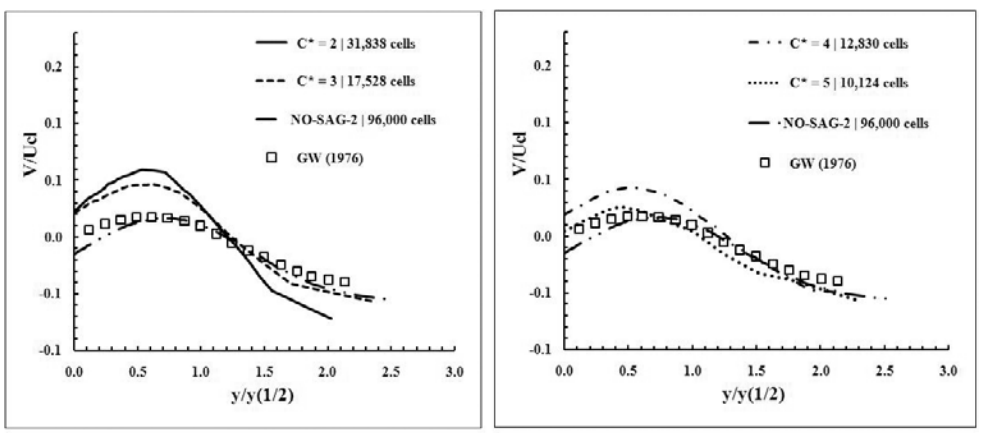

Figure 8. Normalized transverse velocity at x=11D, with different values of C* from left to right.

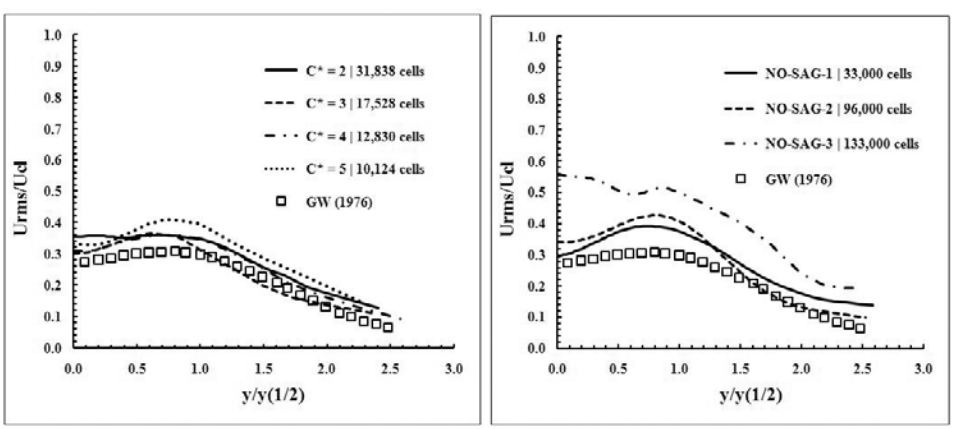

Figure 9. Streamwise fluctuation at x=11D: left) from SAG studies, right) from the conventional mesh cases.

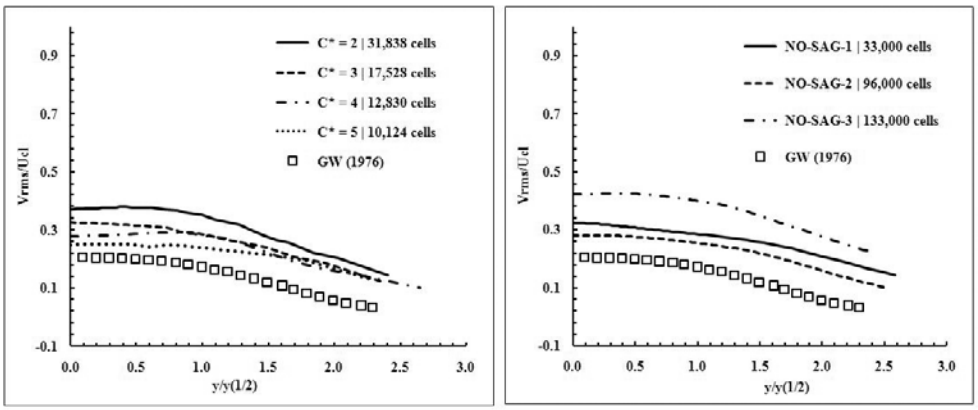

Figure 10. Lateral fluctuation distributions at x=11D: left) from SAG studies, right) from conventional mesh cases.

necessarily a disadvantage, it causes difficulties in separating the contributions of the two errors and consequently makes the evaluation of grid refinement studies difficult too, attempt to validate LES with implicit filtering can also be found in [43]. The results obtained in this work strongly indicate that the location of the smallest resolved grid scales being placed, when adopting the Smagorinsky SGS model, is essential. With the SAG algorithm proposed here, it can be assured that such the smallest resolved grid scales are well placed in the inertial subrange.

For an advantage of using the proposed SAG algorithm in terms of computational requirement, Table 2 gives CPU time in minutes needed to complete one flow-through time, based on U_0 and D. It is clear that the number of grid points (or cells) involved in the calculation is proportional to the amount of computational time needed. With SAG, grid points were added only where necessary and for this study an approximately 10 times less in the number of cells between SAG case with $C^* = 5$ and NO-SAG-2 is evident where both provide the same level of overall result accuracy. This emphasizes the benefit of adopting SAG algorithm in CFD community.

Table 2. CPU time in minutes spent for running one flow-through time (≈ 2,000 time steps) for each case, run on an Intel(R) Xeon(R) computer with 2.66 GHz and 4 GB of RAM.

Case	**Final number of cells [initial mesh: 6,800 cells]**	**CPU time (minutes)**
$C^* = 2$	31,838	42
$C^* = 3$	17,528	35
$C^* = 4$	12,830	22
$C^* = 5$	10,124	19
NO-SAG-1	33,000	51
NO-SAG-2	96,000	94
NO-SAG-3	133,000	147

6. CONCLUSIONS

A new Solution Adaptive Grid (SAG) algorithm is proposed aiming to enhance the efficiency of the SAG methodology in terms of simplicity to define, less user's judgment requirement and computational affordability. The approach is a combination of the real physical turbulent scales namely the Taylor scales and the nature of the Smagorinsky SGS model. The idea was inspired by the uncertainties of mesh refinement application with LES where the grid resolution has an crucial role to play in determining both error sources; numerical and modelling.

The algorithm was applied to a turbulent plane jet in two dimensions and several advantages implicitly and explicitly obtained from this study are:

- It has been emphasized by the results from the conventional mesh cases that in LES, finer mesh does not always lead to better results. This indicates the necessary to have higher mesh density only where needed.
- It can also be concluded that in order to achieve the desired solution with using the Smagorinsky SGS model, the filter width (or the grid size in this case) needs to lie well inside the inertial subrange and with the use of the proposed SAG algorithm the mesh with proper grid size is put accordingly and better results can be expected. Moreover, choices remain for the user to locally vary the smallest grid size by simply changing the refinement variable C^*.
- By increasing the refinement variable C^*, the results are improved. This could be explained by that with coarser mesh the model error is reduced while the numerical error is not significantly changing, or visa versa.
- With a very simple and easy to generate initial mesh, the refinement algorithm is capable of adapting the mesh locally and capture flow effectively leading to improvement in final results. This can have a significant effect in real industrial engineering applications where mesh generation and testing is still a big issue and takes significant engineering time.
- Despite the difficulties in dealing with numerically study of plane jet in two dimensions as common known in literatures, the chosen solver used in conjunction with the proposed mesh adaptation algorithm is proven to give acceptable results.
- With this SAG, a considerable reduction in both computational time and the number of cells required to reach the certain level of accuracy is clearly seen. This strongly suggests the favourably benefit of adopting SAG for CFD problems.
- It is clear that the amount of turbulent intensity at the inlet has strong effect on the flow downstream and without introducing any means of turbulent generator, high mesh resolution is important. It then suggests that with an introduction of turbulent generation to the inlet, further reduction in the degree of freedom can be anticipated.
- Unlike other refinement strategies existing nowadays, the proposed one requires neither mesh density controlling means nor error measurement approximation and moreover, the only additional equation, the refinement variable, is in a very simple form and easy to compute.

REFERENCES

1. Ilinca C, Zhang XD, Trepanier J-Y, Camarero R, A comparison of three error estimation techniques for finite-volume solutions of compressible flows, *Comput. Methods Appl. Mech. Engrg*, 2000, 189: 1277–1294.
2. Zienkiewicz OC, Zhu JZ, A simple error estimator and adaptive procedure for practical engineering analysis, *Int. J. Numer. Meth. Engineering*, 1987, 24: 337–357.

3. Yamaleev NK, Minimization of the truncation error by grid adaptation, *Journal of Computational Physics*, 2001, 170: 459–497.
4. Yamaleev NK., Carpenter MH., On accuracy of adaptive grid methods for captured shocks, *Journal of Computational Physics*, 2002, 181: 280–316.
5. Lohner R., An adaptive finite element scheme for transient problems in CFD, *Comput. Methods Appl. Mech. Engrg*, 1987, 61: 323–338.
6. Warren GP., Anderson WK., Thomas JT., Krist SL., Grid convergence for adaptive methods, *AIAA JOURNAL*, 1991, 91: 1592.
7. Baker TJ., Mesh adaptation strategies for problems in fluid dynamics, *Finite Elements Anal. Design*, 1997, 25: 243.
8. Frey PJ., Alauzet F., Anisotropic mesh adaptation for CFD computations, *Comput. Methods Appl. Mech. Engrg*, 2005, 194: 5068–5082.
9. Habashi WG., Dompierre J., Bourgault Y., Ait-Ali-Yahia D., Fortin M., Vallet M-G., Anisotropic mesh adaptation: towards user-independent, mesh-independent and solver-independent CFD. Part I: general principles, *Int. J. Numer. Meth. Fluids*, 2000, 32: 725–744.
10. Ait-Ali-Yahia D., Habashi WG.,Tam A., Vallet M-G., Fortin M., A directionally adaptive methodology using an edge-based error etimate on quadrilteral grids, *Int. J. Numer. Meth. Fluids*, 1996, 23: 673–690.
11. Habashi WG., Dompierre J., Bourgault Y., Fortin M., Vallet M-G., Certifiable computational fluid dynamics through mesh optimization., *AIAA JOURNAL*, 1998, 36 (5): 703–711.
12. Tam A., Robichaud MP., Tremblay P., Habashi WG., Hohmeyer M., Peeters MF., Guevremont G., Germain P. A 3-D adaptive anisotropic method for external and internal flows. in: *Proceedings of the 36th aerospace sciences meeting*. AIAA 98-00771 Reno, NV 1998.
13. Soni BK., Koomullil R., Thompson D.S., Thornburg H., Solution adaptive grid strategies based onpoint redistribution, *Comput. Methods Appl. Mech. Engrg*, 2000, 189: 1183–1204.
14. Scalabrin LC., Azevedo JLF., Adaptive mesh refinement and coarsening for aerodynamic flow simultations, *Int. J. Numer. Meth. Fluids*, 2004, 45: 1107–1122.
15. Dompierre J., Vallet M-G., Bourgault Y., Fortin M., Habashi WG., Anisotropic mesh adaptation: towards user-independent, mesh-independent and solver-independent CFD solutions: Part III: unstructured meshes, *Int. J. Numer. Meth. Fluids*, 2002, 39: 675–702.
16. Scott McRae D., r-Refinement grid adaptation algorithms and issues, Comput. Methods *Appl. Mech. Engrg*, 2000, 189: 1161–1182.
17. Figueira da Silva LF., Azevedo JLF., Korzenowski H, Unstructured adaptive grid flow simulations of inert and reactive gas mixtures, *J. Comput. Phys*., 2000, 160: 522–540.
18. Popiolek TL., Awruch AM., Numerical simulation of compressible flows using adaptive unstructured meshes and the pseudo-compressibility hypothesis, *Advances in Engineering Software*, 2006, 37: 260–274.
19. Kaennakham S., Holdo AE, The use of solution adaptive grid for low Reynolds number flows, *IJAME*, 2008, 13 (1): to appear.
20. With de G., Holdo AE., Huld TA., The use of dynamic grid adaptation algorithms for the modelling of flow around a cricular cylinder in sub-critical flow regime, *Int. J. Numer. Meth. Fluids*, 2003, 41: 789–808.
21. With de G., Holdo AE., The use of solution adaptive grid for modeling small scale turbulent structures, *ASME*, 2005, 127: 936–944.

22. Hay A., Visonneau M., Adaptive mesh strategy applied to turbulent flows, *C.R. Mecanique*, 2005, 333: 103–110.
23. Ghosal S., An analysis of numerical errors in large -eddy simulations of turbulence, *Journal of Computers and Fluids*, 1996, 125: 187–206.
24. Kravchenko AG., Moin P., On the effect of numerical errors in large eddy simulations of turbulent flows, *Journal of Computers and Fluids*, 1997, 131: 310–322.
25. Vreman B., Geurts B., Kuerten H., Comparison of numerical schemes in large-eddy simulation of the temporal mixing layer, *Int. J. Numer. Methods Fluids*, 1996, 22: 297–311.
26. Geurts Bernard J., *Elements of direct and large-eddy simulation*. Edwards.2004.
27. Schumann U., Subgrid scale model for finite difference simulations of turbulent flows in plane channels annuli, *Journal of Comutational Physics*, 1975, 18: 376–404.
28. Smagorinsky J., General circulation experiment with the primitive equations I. The basic experiment, *Month. Wea. Rev*., 1963, 91: 91–99.
29. Rhie CM., Chow WL., Numerical study of the turbulent flow pas an airfoil with trailing edge separation, *AIAA J*., 1983, 21 (11): 1525–1532.
30. Tennekes H, Lumley JL., *A first course in turbulence*, The Massachusetts Institute of Technology.1972.
31. Dimotakis PE., Turbulent Mixing, *Ann. Rev. Fluid Mech*., 2005, 37: 329–356.
32. Stanley SA, Sarkar S, Mellado JP, A study of the flow-field evolution and mixing in a planar turbulent jet using direct numerical simulation, *J. Fluid Mech*., 2002, 450: 377–407.
33. Klein M., Sadiki A, Janicka J., Investigation of the influence of the Reynolds number on a plane jet using direct numerical simulation, *Int. J. Heat. Fluid Flow*, 2003, 24: 785–794.
34. Ribault C. le, Sarkar S., Stanley SA., Large eddy simulation of a plane jet, *Phys. Fluids*, 1999 11 (10): 3069–3083.
35. Liu Y., Tucker PG., Kerr RM., Linear and nonlinear model large-eddy simulations of a plane jet, *Journal of Computers and Fluids*, 2008, 37: 439–449.
36. Browne LWB, Antonia RA, Rajagopalan S, Chambers AJ. Interaction region of a two-dimensional turbulent plane jet in still air. in: *Structure of complex turbulent shear flows, IUTAM Symposium* Marseille, 1983.
37. Thomas FO, Chu HC., An experimental investigation of the transition of a plannar jet: subharmonic suppression and upstream feedback, *Phys. Fluids*, 1989, A(1): 1566–1587.
38. Gutmark E., Wygnanski I., The planar turbulent jet, *J. Fluid Mech*., 1976, 73 (3): 465–495.
39. Stanley S., Sarkar S., Simulations of spatially developing two-dimensional shear layers and jets, *Theoret. Comput. Fluid Dynamics*, 1997, 9: 121–147.
40. Stanley SA., Sarkar S, Mellado JP., A study of the flow-field evolution and mixing in a planar turbulent jet using direct numerical simulation *J. Fluid Mech*., 2002, 450: 377–407.
41. Goldschmidt VW., Bradshaw P., Effect of nozzle exit turbulence on the spreading (or widening) rate of plane free jets. in: *Joint Engineering, fluid Engineering and Applied Mechanics Conference, ASME* Boulder, Colorado 1981.
42. Klein M., An Attempt to Assess the Quality of Large Eddy Simulation in the Context of Implicit Filtering, *Flow, Turbulence and Combustion*, 2005, 75: 131–147.
43. Celik IB., Cehreli ZN., Yavuz I., Index of resolution quality for large eddy simulations, *Journal of Fluids Engineering*, 2005, 127: 949–959.